Architecture Mapping of the Inner Mitochondrial Membrane Proteome by Chemical Tools in Live Cells

Song-Yi Lee,[†] Myeong-Gyun Kang,[†] Sanghee Shin,[‡,§] Chulhwan Kwak,[†] Taejoon Kwon,[‖] Jeong Kon Seo,*[⊥] Jong-Seo Kim,*[‡,§] and Hyun-Woo Rhee*[†]

[†]Department of Chemistry and [‖]Department of Biomedical Engineering, [⊥]UNIST Central Research Facilities (UCRF), Ulsan National Institute of Science and Technology (UNIST), Ulsan 44919, Korea

[‡]Center for RNA Research, Institute of Basic Science (IBS), Seoul 08826, Korea

[§]School of Biological Sciences, Seoul National University, Seoul 08826, Korea

ⓢ *Supporting Information*
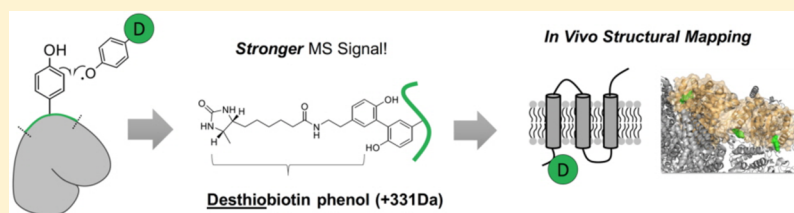
ABSTRACT: The inner mitochondrial membrane (IMM) proteome plays a central role in maintaining mitochondrial physiology and cellular metabolism. Various important biochemical reactions such as oxidative phosphorylation, metabolite production, and mitochondrial biogenesis are conducted by the IMM proteome, and mitochondria-targeted therapeutics have been developed for IMM proteins, which is deeply related for various human metabolic diseases including cancer and neurodegenerative diseases. However, the membrane topology of the IMM proteome remains largely unclear because of the lack of methods to evaluate it in live cells in a high-throughput manner. In this article, we reveal the in vivo topological direction of 135 IMM proteins, using an in situ-generated radical probe with genetically targeted peroxidase (APEX). Owing to the short lifetime of phenoxyl radicals generated in situ by submitochondrial targeted APEX and the impermeability of the IMM to small molecules, the solvent-exposed tyrosine residues of both the matrix and intermembrane space (IMS) sides of IMM proteins were exclusively labeled with the radical probe in live cells by Matrix-APEX and IMS-APEX, respectively and identified by mass spectrometry. From this analysis, we confirmed 58 IMM protein topologies and we could determine the topological direction of 77 IMM proteins whose topology at the IMM has not been fully characterized. We also found several IMM proteins (e.g., LETM1 and OXA1) whose topological information should be revised on the basis of our results. Overall, our identification of structural information on the mitochondrial inner-membrane proteome can provide valuable insights for the architecture and connectome of the IMM proteome in live cells.

INTRODUCTION

The inner mitochondrial membrane (IMM) is one of the most active sites for cellular metabolism.[1,2] The IMM proteome conducts various essential biochemical reactions such as oxidative phosphorylation, metabolite production, and mitochondrial biogenesis. Many IMM proteins form macromolecular complexes at the IMM (e.g., OxPhos complex,[3−6] TIM/TOM complex,[7] MICOS complex,[8] MCU complex,[9] and mitochondrial nucleoid complex[10]), and the IMM proteins in each complex are often coupled with each other to regulate mitochondrial physiology.[11,12] Because abnormal functionality of IMM protein complexes are directly connected to various human metabolic diseases including cancer, diabetes, aging and neurodegenerative diseases,[13−15] it is crucial to understand the correct architecture of the IMM proteome in live cells for efficient development of mitochondria-targeted therapeutics.[16,17] However, there has been no method to reveal the topology of mitochondrial membrane proteins in live cells until now.

Conventional biochemical assays for the topological identification of mitochondrial membrane proteins have been applied only to purified organelle, and the results were often controversial.[18] Furthermore, this method could not be employed in a high-throughput manner. Additionally, several three-dimensional (3D) protein structure analysis methods (e.g., X-ray crystallography and NMR spectroscopy) have been employed only for ultrapurified samples.[3−6] However, these techniques are also limited by the quantity, solubility, and crystallizability of the protein required for the analyses for other membrane protein complexes.[19] Furthermore, all of these in vitro samples are evaluated under nonphysiological conditions; thus, the structures determined by these methods might not
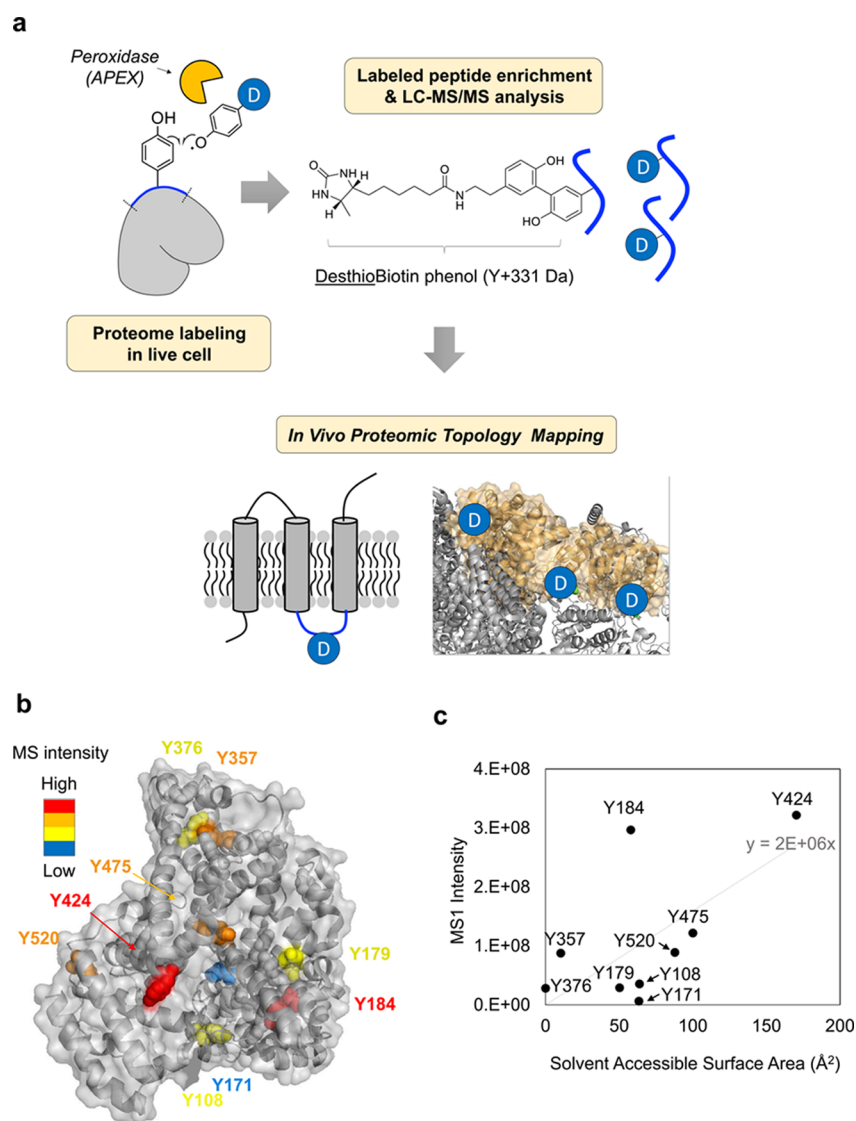
Figure 1. In vivo proteomic topology mapping by LC−MS/MS analysis. (a) Scheme of DBP-labeling method and the identification of labeled site for topology mapping. (b) Mapping of DBP-labeled sites on BSA (PDB ID: 3 V03). The labeled sites are marked with different colors according to the MS1 intensity of the labeled peptides. (c) Correlation graph between solvent accessible surface area (Å², x-axis) and MS1 intensity of labeled peptide per labeled sites on BSA.

perfectly reflect the endogenous protein structure under the heterogeneous conditions of live cells (e.g., protein−protein interactions, post-translational modifications).[20] Thus, another tool that can orthogonally provide in vivo structural information on proteins is required.

In this article, we introduce a new proteomic architecture mapping method by in situ-generated phenoxyl radical probe. Owing to the short lifetime (<1 ms) of phenoxyl radical in aqueous solution,[21] the radical-labeled tyrosine residues may reflect the solvent-exposed sites on the endogenous proteins. Moreover, this radical probe can be in situ generated by genetically targeted peroxidase (APEX) in subcompartmental space of mitochondrion. Thus, the mass spectrometry (MS) identification of labeled tyrosine residues provides topological information on the labeled proteins at each subcompartmental space of the mitochondrion. It is noteworthy that previous analyses by using APEX labeling could not resolve structural identification because these analyses performed based on the unlabeled peptide detection.[21−24]

Topological information can be obtained only by the mass spectrometric analysis of directly modified peptides by phenoxyl radicals. In previous studies, however, only a handful of the labeled peptide were identified mainly due to poor recovery of biotinylated peptides from streptavidin (SA)-beads.[21,22] Consequently, with those lacking number of the labeled sites, a thorough investigation about the correlation between the MS intensity and the solvent exposure level of the labeled peptides could not be carried out. Thus, we designed a new chemical probe, desthiobiotin-phenol that enabled more efficient recovery and stronger MS intensity of the labeled peptides, and applied it to topological mapping of IMM proteome. Our new method resulted in significantly comprehensive identification of labeled sites (Spot-ID) from in situ labeling of mitochondrial matrix and IMM proteome. With the most comprehensive labeled site information so far, we expanded and corrected the topological annotation of mitochondrial membrane proteins, providing a proteomic architecture of IMM proteome in live mammalian cells.

■ RESULTS

Characterization of the Desthiobiotin-phenol (DBP)-Labeling by LC−MS/MS Analysis. The thioether of conventional probe, biotin-phenol (BP), in labeled peptides is easily oxidized to the sulfoxide group during the radical generation reaction,[25,26] which may reduce the signal intensity of the labeled peptides and consequently compromises the identification of low-abundant or inefficiently labeled proteins. In fact, the LC−MS intensity of the oxidized BP-labeled peptides on the tyrosine residue (+377 Da) amounted up to ∼20% of the BP-labeled, original peptides (+361 Da) in human cell lines (Supporting Figure S1). However, the significant sulfur oxidation of BP might be solved by using nonsulfurated biotin or desthiobiotin,[27] as desthiobiotin also has a sufficient binding affinity to SA. Thus, we synthesized desthiobiotin-phenol (DBP) and analyzed its labeled peptides on tyrosine residue (+331 Da) in BSA by LC−MS/MS (Figure 1a). Several DBP-labeled peptides were identified without any further oxidation on DBP, whereas BP-labeled peptides showed an oxidized product at the same sequence (Supporting Figure S1a and Supporting Data Set S1). Notably, LC−MS/MS analysis also indicated that both DBP- and BP-labeled peptides are shown multiple times on the chromatogram, suggesting that heterogeneous products form during the radical coupling reaction (Supporting Figure S1b).

Before SA-enrichment, DBP-labeled peptides showed comparable MS1 intensity to BP-labeled peptides with the identically labeled sites in the 1:1 mixture of BP- and DBP-labeled BSA digests (Supporting Figure S2a). This result indicates that the global labeling efficiency of DBP-labeling is similar to that of BP-labeling. After SA-enrichment, however, the relative intensity of DBP-labeled BSA peptides was enhanced to ∼30% over that of BP-labeled BSA peptides (Supporting Figure S2b), whereas the MS2 response of both labeled peptides with the identical sequence was very similar in terms of fragmentation pattern (Supporting Figure S2c). These results from BSA suggest that the improved MS sensitivity of DBP-labeling might be mainly attributed to the increased elution efficiency of DBP than BP from the SA-beads, not to increased labeling efficiency. The relative affinity difference in both biotin and desthiobiotin to SA also supports this hypothesis. The solid binding affinity ($K_a = 10^{15}$ M^{-1}) of biotin to SA might be too strong to allow detergent-free elution of the biotin-labeled peptides even in the harsh elution condition.[28] However, the lower binding affinity ($K_a = 10^{12}$ M^{-1}) of desthiobiotin toward SA not only appears to be sufficient to bind the labeled peptides to the SA-beads but may also enable the labeled peptides to be easily released from the SA-beads in the detergent-free elution condition (e.g., formamide elution), which is friendly for LC−MS/MS analysis. This result supports that the topology mapping based on the proximity of labeled sites would be practical in proteomic scale using APEX with a DBP probe.

Furthermore, we found there was a positive correlation between the MS1 signal intensity of peptides containing DBP-labeled tyrosine and solvent accessible surface area (SASA, Å^2) of the labeled tyrosine in crystal structure of BSA (Figure 1b and c). Among the labeled tyrosine residues of BSA, we noted solvent-exposed tyrosine residues (Y424, Y475) showed higher MS1 labeling intensity compared with other buried tyrosine residues (Y357, Y376) of BSA. This result implies that DBP radical more efficiently reacts with more exposed tyrosine residues and the MS1 intensity level of labeled peptides can be used for the rough estimation or comparison of solvent exposed surface area of labeled tyrosine. It is noteworthy that Y376, which is completely buried Tyr residue (SASA = 0 Å^2) in BSA crystal structure, was also labeled by DBP (Figure 1b and c). This result suggests that Y376 might be temporally solvent-exposed and could be reacted with DBP radical during dynamic structural changes in solution at room temperature.[29]

Submitochondrial Proteome Mapping by Spot-ID. To investigate the reactivity of DBP with subcellularly expressed APEX in living cells, we treated various APEX2[30] conjugate-expressing cells with BP (500 μM) and DBP (500 μM). As shown in Supporting Figure S3a, BP and DBP generated remarkably similar labeled-protein band patterns, indicating that DBP retains comparable membrane permeability and reactivity with APEX, and its phenoxyl radical efficiently reacted with endogenous proteins as well. To monitor the SA-bead-enrichment property of DBP-labeled proteins, BP- and DBP-labeled proteome by SCO1-APEX2 were analyzed by SA-HRP Western blots before and after enrichment using much more harsh elution condition containing SDS detergent than that condition for LC−MS/MS analysis, in which both the enriched proteome showed similarly strong intensity in SA-HRP Western blots (Supporting Figure S3b). This data confirms that the binding affinity of DBP is practically sufficient for the SA-bead enrichment of labeled protein and the differential LC−MS sensitivity of DBP over BP surely comes from the difference of elution efficiency between the probes on SA-beads, not labeling efficiency, as we described.

Next, the mitochondrial matrix-targeted (Matrix-APEX2) and IMS-targeted LACTB-APEX2 were coupled with DBP-labeling to map the labeled sites (Spot-ID). Previously, these APEX2s were employed for the proteome mapping of submitochondrial spaces based on unlabeled peptide ID; hence, the labeling specificity and the coverage of Spot-ID in our method could be compared with the previous data set.[21,22] Furthermore, we employed a new IMS-targeted APEX2, SCO1-APEX2, which is localized in the IMS and interacting with the cytochrome oxidase complex (Complex IV) as an assembly factor.[31] Thus, we attempted to examine whether SCO1-APEX2 could generate a different set of labeled sites from those of LACTB-APEX2. The expression patterns of Matrix-APEX2, and SCO1-APEX2 were imaged by transmission electron microscope and each DAB/OsO$_4$ staining pattern was well-matched to the expected submitochondrial space (Supporting Figure S4b).[32]

The transiently expressed samples with Matrix-APEX2, LACTB-APEX2, SCO1-APEX2 by Lipofectamine 2000 (L2K) transfection and the untransfected sample were labeled with DBP. From the analysis of this transiently expressed sample analysis, we found not only a distinct cluster of labeled sites from each submitochondrial targeted APEX2 but also a considerable number of labeled peptides from cytosolic proteins, which might be labeled during APEX2 translocation from cytoplasm to the mitochondria (Supporting Figure S4 and Supporting Data Set S2). The labeled sites overlapped between Matrix-APEX2 and IMS-APEX2 are practically important as "background" labeled sites (e.g., CYP51A1) for other APEX-labeled site identifications (see Supporting Information). We expected that these "background" sites could be diminished when APEX expression and the concentration of DBP would be stringently controlled at low levels in stable cell lines for less spurious phenoxyl radical labeling.
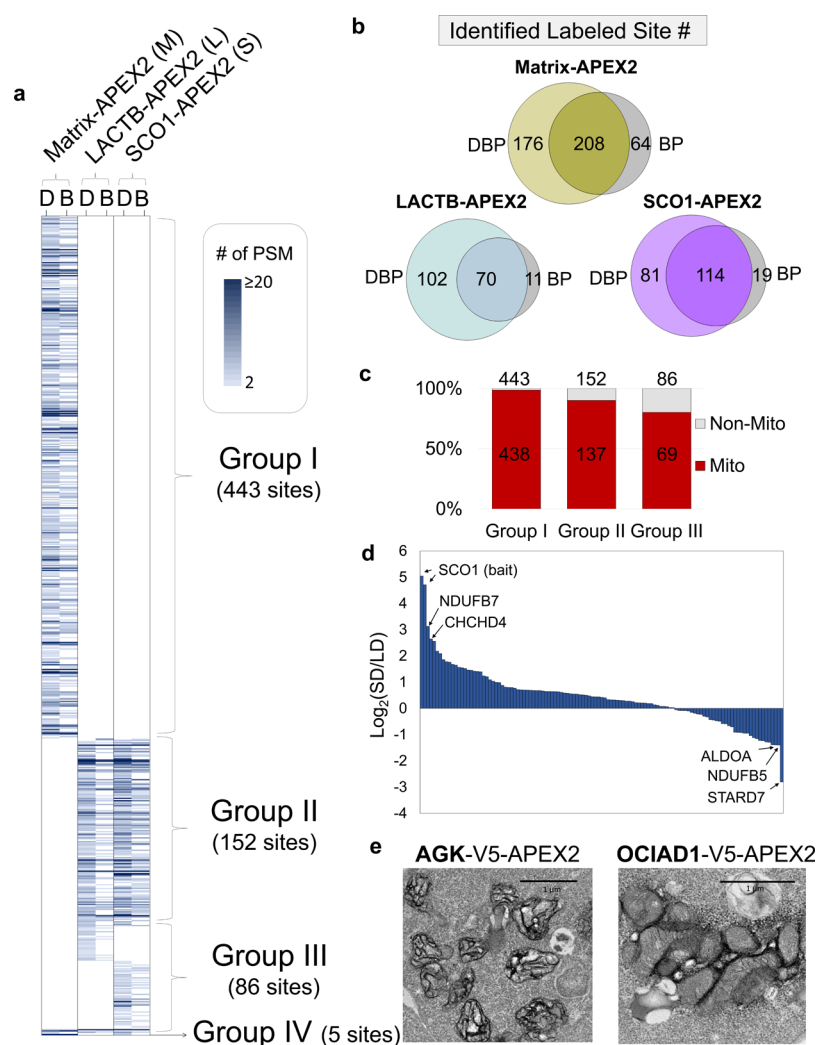
Figure 2. Identified DBP-labeled sites by APEX2. (a) Overview of 686 DBP- and BP-labeled sites of mitochondrial Matrix-APEX2, LACTB-APEX2 and SCO1-APEX2 stable cell lines. The table shows the findings for each reproducibly labeled site per biological replicate experiment. The color intensity represents number of peptide spectra match (PSM) of the labeled peptides per unique labeled site over replicate experiments with various APEX2s. Detailed information is shown in the Supporting Data Set S3. (b) Overlaps of identified DBP- and BP-labeled unique sites in parallel experiments for Matrix-, LACTB-, and SCO1-APEXs. (c) Mitochondrial specificity check of Groups I to III. The number of total labeled sites is depicted over the column. (d) Differential MS1 intensity of respectively labeled peptide between SCO1- and LACTB-APEX2 sample. x-axis: labeled site, y-axis: log2 value of differential peptide MS1 intensity of SCO1 (S) over LACTB (L). (e) Electron microscopic imaging of AGK-V5-APEX2 and OCIAD1-V5-APEX2. Scale bar: 1 μm.

We generated Flp-In T-REx 293 stable cell lines with Matrix-APEX2, LACTB-APEX2, and SCO1-APEX2 and performed Spot-ID with these cell lines. Labeled sites were assigned when they were reproducibly observed in each biological replicate. From the analysis of DBP-labeled peptides from six independently labeled samples, we identified 608 unique DBP-labeled sites, which were reproducibly discovered in each replicate of APEX2-labeled samples. We also confirmed that DBP showed better depth of coverage (e.g., peptide spectrum match and unique labeled site number) than by using the previous probe (BP) in the parallel experiments by using Matrix-APEX2, LACTB-APEX2 and SCO1-APEX2 (Figure 2b and Supporting Data Set S3). We clustered four exclusively labeled sets (Groups I−IV) of DBP- and BP-labeled tyrosine residues (total 686 sites) from the three APEX2s results (Figure 2a, Supporting Data Set S3). Group I sites (443 sites) were exclusively labeled only by Matrix-APEX2, and Group II sites (152 sites) were labeled by both LACTB-APEX2 and SCO1-

APEX2, but not by Matrix-APEX2. Over 98% of Group I and over 90% Group II sites were mapped on the mitochondrial proteins with high mito-specificity (Figure 2c).

Furthermore, the majority of Group I's mitochondrial proteins were mapped onto mitochondrial matrix or IMM proteins (Supporting Data Set S3). Only two IMS proteins, PNPT1 (also known as PNPase)[33] and STOML2[34] were assigned to Group I. However, PNPT1 has been recently reidentified as a mitochondrial matrix protein with supporting evidence of EM imaging in the previous study.[21] Since we could not find any labeled sites of STOML2 by IMS-APEX2, this peripheral membrane protein should be localized in the mitochondrial matrix. In contrast, we found two matrix proteins (NDUFA4 and NDUFB10, known as matrix-side subunits of OxPhos Complex,[35,36]) were reproducibly labeled by IMS-APEX2 (Group II, Supporting Data Set S3). From the immunoprecipitation experiment, we confirmed that NDUFB10 and STOML2 were exclusively DBP-modified in

IMS- and Matrix-APEX2 sample, respectively (Supporting Figure S5a). This result indicates that our MS-identification of these proteins based on the modification site is not false positive. Because NDUFA4, NDUFB10 and STOML2 contain no predicted transmembrane domain, their submitochondrial localization should be revised according to their labeled sites by APEXs.

We also found that CLPB, a known mitochondrial matrix chaperone protein,[37] were exclusively labeled by IMS-APEX2. For confirmation of CLPB's localization in mitochondrion, we prepared CLPB-APEX2 and examined its biotinylation pattern which can tell its submitochondrial localization.[38] We could observe very diffusive biotinylated pattern of CLPB-APEX2 from mitochondria, which supports that CLPB should not be localized within the mitochondrial matrix (Supporting Figure S5b). Furthermore, analysis of correlations between CLPB-APEX2's biotinylated protein pattern with that of other standard submitochondrial-targeted APEX2 constructs (e.g., Matrix, SCO1 and TOM20-APEX2s), using Western blot with SA-HRP (Supporting Figure S5c and d) revealed a high correlation with the pattern observed with SCO1 (0.89) and low correlations with TOM20 (0.64) and Matrix (0.67), indicating that the CLPB C-terminus localized to the IMS (Supporting Figure S5e). Thus, our data suggest that CLPB should be located at IMS and its function as molecular chaperone should be rediscussed in the IMS not in the mitochondrial matrix.[37]

A distinct cluster of labeled sites by either LACTB-APEX2 (28 sites) or SCO1-APEX2 (58 sites) was also detected in Group III (Figure 2a). LACTB-APEX2 exclusively labeled more number of cytosolic proteins (e.g., YBX1, YWHAQ), whereas SCO1-APEX2 labeled inner mitochondrial membrane proteins such as OPA1, TIMM17B and MICU1. Among the respectively DBP-labeled peptides by SCO1-APEX2 and LACTB-APEX2 in Group II, several peptides showed distinctively differential MS1 signal intensities (Figure 2d). For example, SCO1 (bait, Y216, Y244), NDUFB7 (Y89) and CHCHD4/MIA40 (Y105) PTGES2 (Y263) and AIFM1 (Y347) showed reproducibly higher MS1 intensity in SCO1-APEX2 than LACTB-APEX2, whereas STARD7 (Y171), NDUFB5 (Y171) and ALDOA (Y364) showed higher MS1 intensity in LACTB-APEX2 than SCO1-APEX2. Since the stronger MS1 signal intensity should be originated from more efficient DBP labeling which is dependent on proximity, we postulated that these differentially labeled proteins including exclusively labeled proteins might be considered as a clustered proteome that is proximal to SCO1-APEX2 or to LACTB-APEX2 in IMS.

Among the labeled proteins by IMS-APEXs (LACTB-APEX2 or SCO1-APEX2), we found several mito-orphan proteins (e.g., ACOT1, SMIM4 and TMEM223, Supporting Data Set S3) and a considerable number of mitochondrial proteins still have no any submitochondrial annotation, which were labeled either by Matrix-APEX2 (Matrix-orphan, Supporting Data Set S3) or IMS-APEX2 (IMS-orphan, Supporting Data Set S3). For example, AGK is known as a mitochondrial protein without submitochondrial annotation and it is exclusively labeled by IMS-APEX2, which suggests that AGK should be an IMS protein or at least an IMS-exposed domain containing protein.

For the confirmation of their submitochondrial location, AGK-V5-APEX2 and OCIAD1-V5-APEX2 (C-term tagged APEX2 at the target protein) were constructed and used for imaging by electron microscope (EM). The EM images showed

that AGK-V5-APEX2 was clearly localized to IMS, while OCAID1-V5-APEX2 was localized to outer mitochondrial membrane (OMM) (Figure 2e), indicating its C-terminus headed for OMM. Considering the labeled sites (Y25, Y128, Y129, Y199, Y210) of OCIAD1 by IMS-APEX2, we postulated that OCIAD1 should contain plausible transmembrane domain through OMM.

TMEM261 Is a Newly Identified Mitochondrial Protein in IMS. Notably, we reproducibly found DBP-labeled Y12 of TMEM261 (also known as C9orf123) in LACTB-APEX2 and SCO1-APEX2 samples, which is a transmembrane (TM) protein without subcellular annotation. To confirm its subcellular localization, we cloned TMEM261-V5-APEX2 and checked its expression and biotin-labeled pattern. Although this protein is not currently annotated as a mitochondrial protein,[39] TMEM261-V5-APEX2 showed a clear mitochondrial pattern, which overlaid well with the mitochondrial marker protein, mito-BFP (Figure 3a). Furthermore, its biotinylation pattern was not restricted to mitochondria, indicating the biotinylated proteins by TMEM261-APEX2 were diffused from the porous outer mitochondrial membrane and this result implies that C-terminus of TMEM261 might be localized to IMS or OMM.[38] We also performed transmission electron microscopy (TEM) imaging of TMEM261-V5-APEX2, which clearly localized in IMS (Figure 3b). This result indicates that the C-terminus of TMEM261 is exposed in the IMS (Figure 3c). Considering its two expected TM domains, the labeled site (Y12) by IMS-APEX2 and EM imaging result of C-term tagged APEX2 at TMEM261-APEX2, TMEM261 is likely to be an IMM or OMM protein, with its N- and C-terminus exposed to the IMS (Figure 3c).

To understand its role in the mitochondria, we also performed Spot-ID experiments with TMEM261-APEX2 stable cell line. We collected 470 DBP-labeled sites in TMEM261-APEX2 (Supporting Data Set S4) and among these labeled sites, ∼39% of sites (182 sites) were overlapped with labeled sites of IMS-APEX2 (Group II, Figure 3d). In this analysis, we could observe again that DBP showed much better depth of coverage of labeled sites (total 470 sites) than by using the previous probe (BP, total 284 sites) in the parallel experiments (Figure 3e and Supporting Data Set S4). Interestingly, distinctly labeled sites of endoplasmic reticulum (ER) lumen or secretory pathway proteins such as CALU, RCN1, RCN2, HSP90B1, PDIA3, and PDIA6 were observed in its exclusively labeled sites of TMEM261-APEX2 (Group III, Figure 3d and f). The labeled sites of these ER lumen proteins were not covered by other IMS-APEX2s or Matrix-APEX2. In further analysis, these labeled sites on ER-lumen proteins were also identified by ss-APEX2-KDEL whose APEX2 is localized at the ER lumen, whereas these labeled sites were not covered by APEX2-NES whose APEX2 is localized at the cytoplasm (Supporting Data Set S5). This result implies that TMEM261 might be very proximate to the ER-mitochondrion tethered junction;[40,41] thus, its generated DBP radical can diffuse efficiently into the ER lumen through OMM (Figure 3g). We also found that several DBP-labeled nuclear proteins (e.g., DDX3X and RUVBL1) in Group III have known mitochondrial functions.[42,43] Thus, it might be intriguing to investigate whether functions of nuclear proteins labeled by TMEM261-APEX2 are related to mitochondria and nuclear crosstalk[44,45] in future studies.

Interestingly, a recent report suggested this gene is significantly overexpressed in human breast cancer in the

Figure 3. continued

information is shown in the Supporting Data Set S4. (e) Overlaps of identified DBP- and BP-labeled unique sites in parallel experiments for TMEM261-APEX2. (f) Suborganelle specificity of labeled sites in Group II and Group III. The number of total identified sites with subcellular information is depicted over the column. (g) Schematic representation of TMEM261 localization in IMS near the ER-mitochondrial junction based on the Spot-ID result.

context of gene copy number amplification.[46] Moreover, we found the possibility of TMEM261 as an oncogene in prostate cancer from bioinformatics analysis (Supporting Information). Thus, further study is required to investigate its physiological role related to mitochondrial function in cancer tissues in the future.

In Vivo Membrane Protein Topology Determination by Spot-ID. Our Spot-ID results provided valuable information on the topological direction of membrane proteins; due to the short lifetime of in situ-generated phenoxyl radicals and the high impermeability property of the IMM, the labeled sites should be in the same direction as that of targeted APEX. For instance, MIC60/IMMT (also known as mitofilin) is a core IMM protein component of the MICOS complex,[47] and the N-terminus domain (1−46 aa) is localized in the matrix, and the C-terminus domain (65−758 aa) is localized in the IMS. The 33rd tyrosine residue of MIC60 was labeled by Matrix-APEX2 (Group I), and the 95th, 358th, 543rd and 578th tyrosine residues of MIC60 were labeled by IMS-APEX2s (Group II and III) (Figure 4a). The topological direction of 16 TM including MIC60 proteins at IMM were also well-matched with labeled sites either by Matrix-APEX2 or IMS-APEX2 (SCO1-APEX2 and LACTB-APEX2) (Figure 4b and Supporting Figure S6a). For peripheral membrane proteins, 26 matrix-localized proteins were exclusively labeled by Matrix-APEX2, and 16 IMS-localized proteins were exclusively labeled by IMS-APEX2s (Figure 4c and Supporting Figure S7a). Given that our labeled site accurately reflected its sublocalized spaces, we determined the topology of 44 mitochondrial TM proteins at the IMM (Figure 4d, h and Supporting Figure S6b) and membrane-localized direction of 33 mitochondrial peripheral membrane proteins at the IMM (Figure 4e, h and Supporting Figure S7b).

Interestingly, we found that Y17 of UQCRQ was reproducibly labeled by Matrix-APEX2 while Y60 and Y78 of UQCRQ was reproducibly labeled by IMS-APEX2. Although UQCRQ contains no reported TM domain in Uniprot, our results strongly suggest that UQCRQ should be a TM protein at the IMM. Similarly, we also found Y38 of COX4I1 was labeled by Matrix-APEX2, whereas Y126 of COX4I1 was labeled by IMS-APEX2. This result also suggests that COX4I1 should have a single TM domain between 38 and 126 aa at IMM. It is noteworthy that the Dense Alignment Surface (DAS)-TM analysis[48] predicted a single transmembrane domain for both COX4I1 and UQCRQ, consistent with our result (Supporting Figure S6c and d). The proposed topologies of these proteins are shown in Figure 4d.

Among the labeled sites, we observed several OMM proteins labeled by IMS-APEX2. For example, MUL1, an OMM transmembrane protein with both N- and C-termini exposed to the cytosol,[49] was labeled by IMS-APEX2 at Y173, which is exposed to IMS (Figure 4f). We also found that several beta-barrel OMM proteins such as VDAC1, VDAC2, VDAC3, and SAMM50 were labeled by IMS-APEX2. Intriguingly, all four
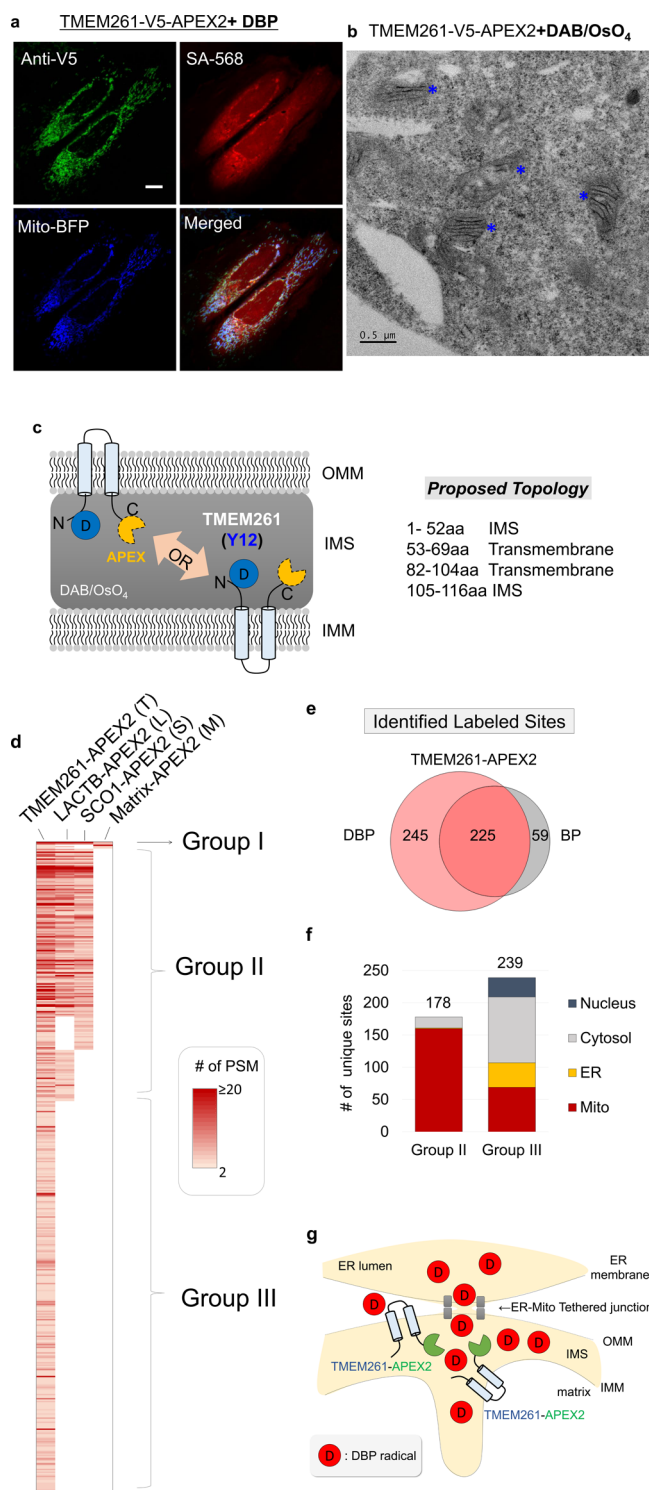
Figure 3. TMEM261 is a newly identified mitochondrial protein. (a) TMEM261-V5-APEX2 labeling imaging; the green channel (anti-V5) is for enzyme expression pattern; the red channel (SA-568), for the DBP labeling pattern; and the blue channel is for the mitochondrial marker mito-BFP. HeLa cell was used for this imaging experiment. Scale bar = 10 μm. (b) Electron microscopic imaging of TMEM261-V5-APEX2. TMEM261-V5-APEX2 labeling sites are depicted by blue asterisks. Scale bar: 500 nm. (c) The proposed membrane topology of TMEM261 in the mitochondrion. (d) Overview of 470 DBP-labeled sites of TMEM261-APEX2. The table shows the findings of each reproducibly labeled site per biological replicate experiment. The color intensity represents number of peptide spectra match of the labeled peptides per unique labeled site over replicate experiments. Detailed
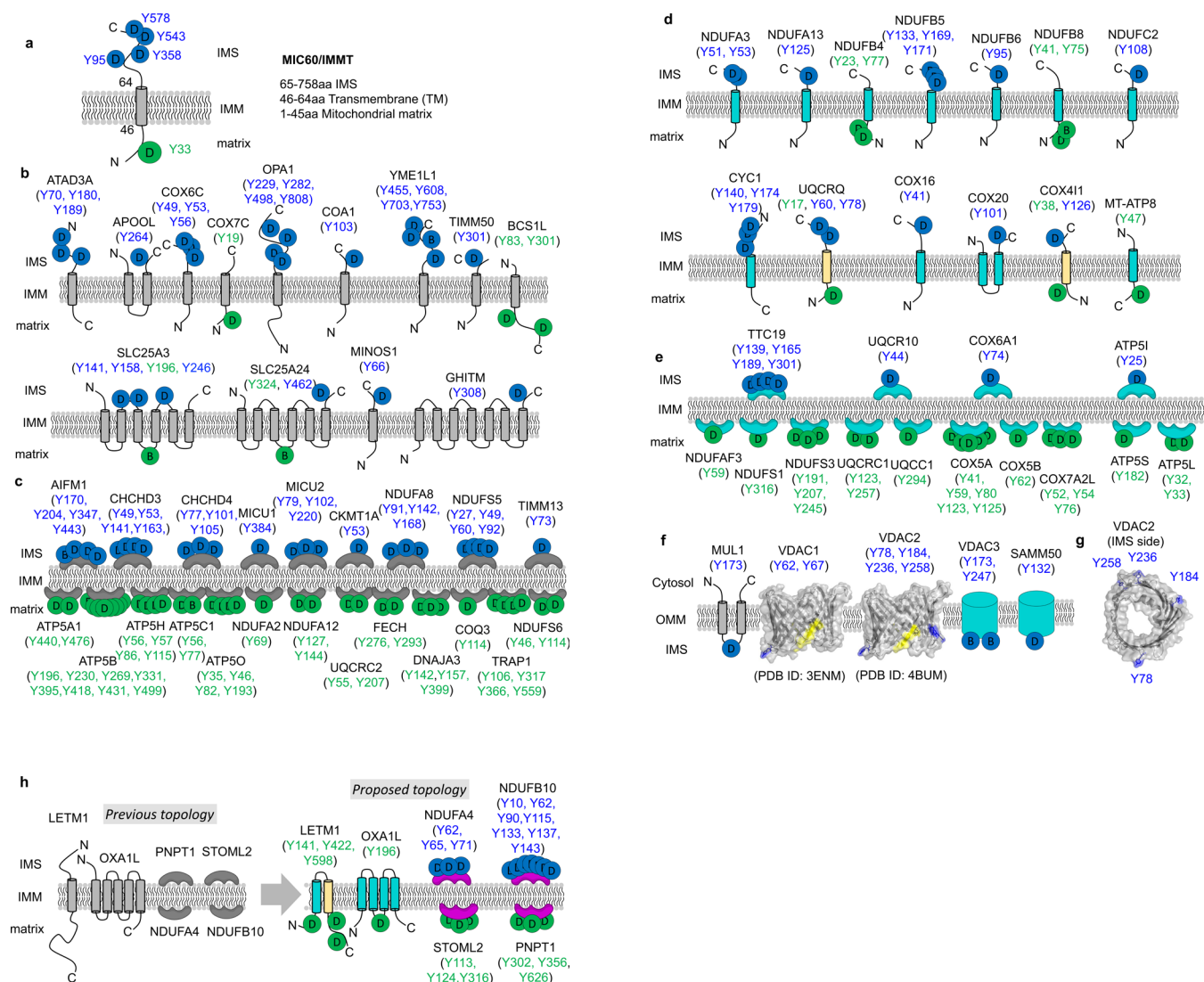
Figure 4. Labeled sites for in vivo protein topology determination. (a) MIC60/IMMT protein topology confirmation by our labeled sites. (b) IMM-TM protein topology confirmation. Other confirmed IMM-TM proteins are shown in Supporting Figure S6a. (c) Peripheral membrane protein-binding face confirmation by our results. Other confirmed IMM-peripheral membrane proteins are shown in Supporting Figure S7a. (d) Proposed membrane topology of IMM-TM proteins of OxPhos complex by our labeled site result. Other proposed IMM-TM proteins are shown in Supporting Figure S6b. (e) Proposed membrane-binding face of several peripheral membrane OxPhos complex proteins at the IMM based on the labeled sites. Other proposed IMM-peripheral membrane proteins are shown in Supporting Figure S7b. (f) Confirmed and proposed orientation of OMM proteins based on the sites labeled by IMS-APEX2. N- and C-termini of VDAC1 (PDB ID: 3ENM) and VDAC2 (PDB ID: 4BUM) are shown in yellow, and tyrosine residues labeled by IMS-APEX2 are in blue. (g) IMS side of VDAC2 protein. (h) Proposed membrane topology of LETM1, OXA1L, STOML2, NDUFA4, and NDUFB10 by our labeled site results. The proposed TM direction is shown in blue. The proposed newly identified TM domain is shown in yellow. Either DBP- or BP-labeled sites by Matrix-APEX2 are marked by green circles with "D" or "B" respectively, and DBP- or BP-labeled sites by IMS-APEX2 are marked with blue circles with "D" or "B" respectively. Detailed information is shown in the Supporting Data Set S3.

DBP-labeled tyrosine residues (Y78, Y184, Y236, and Y258) of VDAC2 were positioned at the same side of the protein (Figure 4f and g), indicating that this side of VDAC2 is exposed to IMS. Additionally, we could determine that the N- and C-termini of VDAC1 were exposed to IMS based on the labeled site (Y62, Y67). Our data proposed that these two VDAC proteins have the same orientation based on the sites labeled by IMS-APEX2 (Figure 4f). Considering that the orientation of VDAC protein is still under debate,[50] it is noteworthy that our proposed orientation of VDAC1 is consistent with the previously determined orientation of tagged VDAC1[51,52] and a dynamic simulation study of VDAC1.[53] Similarly, for the first time, we proposed the orientation of VDAC3[54] and SAMM50[55] at

OMM based on our labeled sites. Furthermore, the labeled sites of VDAC1 and VDAC2 in our data set, which are located at the same side of the structure, supports that these crystal structures of VDAC1[56] and VDAC2[57] are close to their native conformation in live cells.[58]

We also found some results conflicting with previously established topologies of IMM membrane proteins such as LETM1 (Uniprot ID: O95202)[59] and OXA1L (Uniprot ID: Q15070).[60] To confirm that the N-terminus domain of LETM1 containing Y141 is exposed in the mitochondrial matrix, we prepared a V5-APEX2-LETM1 construct, in which APEX2 is inserted between 151-aa and 152-aa of LETM1 (Supporting Figure S8a). We checked the expressed and biotinylated
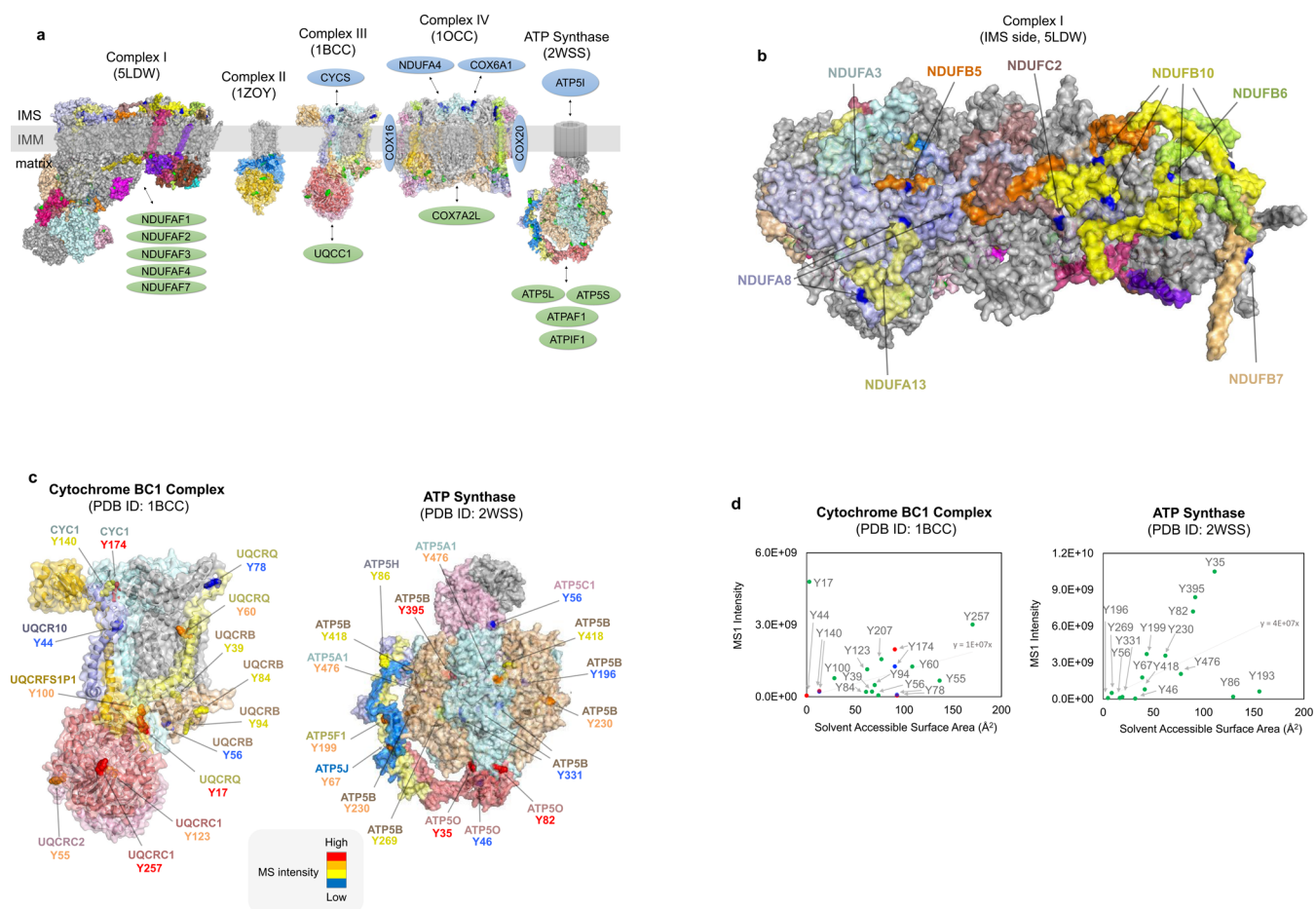
Figure 5. Labeled sites on the OxPhos complex. (a) Crystal or EM structures of Complex I (PDB ID: 5LDW), Complex II (PDB ID: 1ZOY), Complex III (PDB ID: 1BCC), Complex IV (PDB ID: 1OCC), and ATP synthase (PDB ID: 2WSS). The MS-identified subunits were colored with different colors, the tyrosine residues labeled by Matrix-APEX2 were colored in green, and the residues labeled by IMS-APEX2 were colored in blue. The supernumerary subunits of OxPhos complex that were not characterized by the crystal or EM structures but were identified by either Matrix-APEX2 or IMS-APEX2 are shown. (b) IMS side of Complex I (PDB ID: 5LDW). Labeled IMS-side-exposed subunits of Complex I are colored with various colors and the sites labeled by IMS-APEX2 are colored in blue. The sites labeled by Matrix-APEX2 were shown in Supporting Figure S10. (c) Cytochrome BC1 complex (Complex III, left) and mitochondrial ATP synthase complex (right). The labeled sites are marked with different colors according to the MS1 intensity of the labeled peptides. (d) Correlation between solvent-accessible surface area (Å^2, x-axis) and MS1 intensity of labeled peptides per labeled site on the crystal structures shown in (c). The sites labeled by Matrix-APEX2 are colored in green and those by SCO1-APEX2 or LACTB-APEX2 are colored in red or blue, respectively. Correlation factor was included in the graph. When the labeled sites are shown in multiple times at identical chains, the highest solvent accessible surface area among the identical sites was selected for this graph Detailed information on the labeled subunits and labeled residues of theses mitochondrial complexes were shown in Supporting Data Set S6.

patterns in HEK293T cells, and it showed a good mitochondrial pattern and very restricted biotinylated pattern (Supporting Figure S8b), which implies APEX2 in this construct should be positioned in the mitochondrial matrix.[38] In addition, we performed EM imaging[32] of V5-APEX2-LETM1, which very clearly showed mitochondrial matrix staining (Supporting Figure S8c and d). Thus, we can correct that LETM1's N-terminus stretched out to the matrix, not to IMS, which concurs with its labeled site (Y141) by Matrix-APEX2. When considering the two predicted TM domains (204−232 aa and 413−421 aa, Supporting Figure S8e) along with its DBP-labeled sites (Y141, Y422, Y598) by Matrix-APEX2, we propose that LETM1 exhibits the membrane topology shown in Supporting Figure S8f.

Interestingly, the DAS-TM prediction program also indicates that OXA1L may contain 4 TM domains (Supporting Figure S9a), whereas 5 annotated TM domains are shown in Uniprot. The number of TM domains is important in membrane topology because the odd or even number of TM domains

indicates cross-membrane localization or colocalization of N- and C-termini of OXA1L, respectively. Thus, we sought to determine whether OXA1L's N-terminal and C-terminal domains localized to the mitochondrial matrix by APEX-EM.[61] For this, we prepared OXA1L(1−435 aa)-V5-APEX2 where V5-APEX2 was conjugated to the C-terminus of full-length OXA1L (Supporting Figure S9b). Notably, APEX-EM imaging showed clear mitochondrial matrix staining (Supporting Figure S9c). This finding was subsequently confirmed by bioinformatics analysis with Mitoprot,[62] which predicted that N-terminal domain of OXA1L (1−72 aa) harbors a strong mitochondrial targeting sequence with over 97% confidence that would be cleaved after mitochondrial translocation. Following this result, we prepared OXA1L(1−73 aa)-V5-APEX2 where V5-APEX2 was conjugated to the C-terminus of the N-terminal OXA1L(1−73 aa) domain construct (Supporting Figure S9b) and found obvious mitochondrial matrix localization with APEX2-EM (Supporting Figure S9d). Thus, EM imaging with Spot-ID results (Y196) proposed a topology

with 4 TM domains (Supporting Figure S9e). We also identified that cleavage of OXA1L N-terminal signal peptide (1−72aa) occurred by Western blotting (Supporting Figure S9f). Our proposed topology of LETM1 and other membrane proteins (OXA1L, PNPT1, STOML2, NDUFA4, and NDUFB10) are displayed in Figure 4h.

In Vivo Structural Identification of Mitochondrial Protein by Spot-ID. In our data set, numerous tyrosine residues of OxPhos subunits were identified as labeled sites by Matrix- or IMS-APEX2. On the basis of the resulting labeling information in matrix or in IMS, the orientation of these subunits was proposed (Figure 4). Our proposed topology of the OxPhos complex is consistent with the crystal or EM structure of these complexes (Figure 5). For example, Complex I in mammalian mitochondria, whose structure was recently reported by the Hirst group,[6] comprises 45 proteins, including 31 supernumerary subunits. Among these proteins, 21 proteins were mapped by both Matrix- and IMS-APEX2, and their labeled sites exactly matched either matrix-side or IMS-side exposed tyrosine residues on the complex (Figure 5a). Interestingly, NDUFB10, which was annotated as a matrix protein in Uniprot but was labeled by IMS-APEX2 in our data, was positioned at the IMS side in a recently reported Complex I structure (Figure 5b).[6] In other mitochondrial complexes (e.g., Complex II, III, and IV and ATP Synthase),[3−5,63] the discovered labeled sites were well-matched with the determined protein structure in terms of the orientation of the tyrosine residue at IMM (Figure 5 and Supporting Figure S10). Given that some of our identified protein topology of OxPhos complex subunits are indeed well-supported by identified crystal structures of OxPhos complex, our proposed membrane topologies of other IMM and OMM proteins should be considered as a true positive resource (Supporting Data Set S7).

We also found that the labeled sites were primarily localized at the surface-exposed subunits of the complexes. For instance, none of the core membrane subunit proteins (e.g., ND1, ND2, ND3, and ND4) of Complex I were labeled by either APEX, but the supernumerary subunits (e.g., NDUFA3, NDUFA8, NDUFA13, NDUFAB1, NDUFB4, NDUFB5, NDUFB6, NDUFB7, NDUFB8, NDUFB9, NDUFB10, and NDUFC2), which are components for building a cage structure around the core membrane subunits, were found to be labeled by APEX2 (Figure 5b and Supporting Figure S10). This result indicates that the solvent-accessible protein subunits were preferentially labeled by APEX over the structurally buried protein subunits in the complex. There are several supernumerary subunits of OxPhos complex that were not characterized by the atomic structures but identified in our study. The topological direction of those accessory subunits (e.g., NDUFAF1, NDUFAF2, NDUFAF3, NDUFAF4, NDUFAF7, TIMMDC1/C3orf1, TMEM126B for Complex I; UQCC1 for Complex II; TTC19 for Complex III, NDUFA4, COX6A1, COX7A2L, SCO1, SCO2, CMC2, TACO1, LRPPRC for Complex IV; ATP5I, ATP5L, ATP5S, ATPAF1, ATPAI1 for ATP Synthase) are proposed in Figure 5a and Supporting Figure S11.

As we described in Figure 1c, the short-lived phenoxyl radical tends to react on the protein surface tyrosine residue in a simple in vitro experiment. We further examined a correlation between the surface exposure level and the MS intensity of labeled peptides in the living cells by matching several identified sites with the crystal structure of mitochondrial macromolecular protein complexes. As shown in Figure 5, we marked the

identified tyrosine residues on the ATP Synthase and cytochrome BC1 complex (also known as Complex III) with differential color codes according to the MS1 intensity (Figure 5c). We observed that more exposed residues (e.g., Y35 and Y82 of ATP5O; Y257 of UQCRC1) were more strongly labeled than other tyrosine residues. In this macromolecular complex, a positive correlation between MS1 signal intensity of the labeled sites and its exposure level (solvent accessible surface area, $Å^2$) was also observed (Figure 5d). Interestingly, a couple of the labeled sites with considerably high MS1 intensity were not fully exposed on the surface. For example, Y17 of UQCRQ possesses a negligible solvent accessible surface area (2.7 $Å^2$) in the crystal structure, however, its labeled peptide showed the highest MS1 intensity (4.8 × 10^8) among the labeled tyrosine residues of cytochrome BC complex. Since the protein structure can be dynamically changed by interaction with other proteins or post-translational modification, we postulated that this site might be exposed to solvent in their dynamic native structure and followed by phenoxyl radical labeling. Thus, we postulated that the MS intensity of our Spot-ID peptides can reflect the native dynamic structure of protein in a living cellular context.[64,65]

■ DISCUSSION

We found our proposed topologies of mitochondrial membrane proteins can provide insights for physically interacting domain within certain mitochondrial complexes. For example, it was reported that OXA1L interacted with mitochondrial ribosome in the matrix with its C-terminus;[60] however, our identified topologies of OXA1L propose that its N-terminus should interact with mitochondrial ribosome (Supporting Figure S12). Because OXA1L plays a major role in nuclear-encoded protein translocation from the cytosol,[66] our result supports that C-terminus of OXA1L should interact with its substrate proteins at the IMS side. Interestingly, our proposed topologies of PHB (IMS-side) and STOML2 (matrix-side) hypothesizes whether these two protein interaction[34] should be mediated by a IMM-TM protein (e.g., ATAD3A) at IMM. Our proposed connectome of protein subunits in other mitochondrial macromolecular complexes at IMM (e.g., TIM23 complex, MICOS complex, PHB complex) are shown in Supporting Figure S12.

Compared to previous identification results based on SILAC ratio of the unlabeled peptides,[21,22] our Spot-ID approach showed lower numbers of identified proteins (Supporting Figure S13b); however, previously identified results contain false positives due to the indirect determination of proximity labeled proteins, as we described. For example, CHCHD3 is a mitochondrial peripheral membrane protein at IMS-side, however, it was previously identified as a mitochondrial matrix protein by Matrix-APEX.[21] In current study, we did not observe any labeled peptide of CHCHD3 reported by Matrix-APEX2, while multiple labeled peptides of CHCHD3 were detected by LACTB-, SCO1-, or TMEM261-APEX2s, with strong MS1 intensity. From the immunoprecipitation experiment, we confirmed that CHCHD3 was not labeled in the Matrix-APEX2 sample, whereas it was strongly labeled by either LACTB-APEX2 or SCO1-APEX2 (Supporting Figure S13c). It is possible that CHCHD3 was mis-annotated as a matrix protein in previous study via the strong interaction with biotinylated transmembrane protein (e.g., MIC60)[67] at the matrix-side by Matrix-APEX (Supporting Figure S13d). Likewise other peripheral IMM proteins (e.g., ATP5J, COX5A and

COX5B) with labeled sites from Matrix-APEX2 in this study, but previously annotated as IMS proteins,[22] should be regarded as matrix proteins. Overall, this analysis supports that our proposed submitochondrial localization of ~250 mito-orphan proteins should be considered as a true resource for the spatial-resolved clustered proteome within the mitochondrion (Supporting Data Set S3). We also found that the coverage of labeled peptides by Spot-ID workflow with DBP (Supporting Figure S13e) were significantly higher than that of previously identified BP-labeled peptides with low false discovery rate (Supporting Figure S13).

The MS signal enhancement after enrichment in DBP-labeling over BP-labeling was observed in APEX2-labeled human cell line sample. The MS signal gain of DBP-labeled peptides was ranging up to >10-fold higher than that of BP-labeled peptides for ~80% of labeled peptides and was not dependent on protein abundance (Supporting Figure S14a). Overall, the DBP-labeling clearly resulted in a higher number of identified spectra (+35−97%), and unique labeled sites (+41−112%) than BP-labeling method in human cell lines (Supporting Figure S14b). In addition, the MS signal intensity of the DBP-labeled peptides was highly reproducible between the replicates (Supporting Figure S14c).

We also performed a Spot-ID analysis by using ss-APEX2-KDEL and found that various ER luminal proteins were labeled by this construct (Supporting Figure S15 and Supporting Data Set S5). This result indicates that our DBP-APEX method universally works in other subcellular compartments, in contrast to other proximity labeling methods using promiscuous biotin ligase (pBirA), which is less active in the secretory pathway.[21] Compared with the same mitochondrial targeting sequence of Matrix-APEX2, we also found that translocation of pBirA to the mitochondrial matrix was not efficient (Supporting Figure S16). Other in vivo membrane topology identification methods using enzymatic glycosylation[68] are limited to the secretory pathway and cannot be employed in other subcellular spaces such as the mitochondrion.

Notably, conventional biochemical analysis by proteinase K digestion and digitonin treatment showed that NDUFB10 and STOML2 localized to the mitochondrial matrix and IMS, repectively, and this results are inconsistent with that determined by Spot-ID (Supporting Figure S17). However, the recently characterized Complex I[6] atomic structure provided clear evidence that NDUFB10 is located in the IMS. In addition, the proteinase K/digitonin preparation method may have also resulted in incorrect conclusions on the number of transmembrane domains in OXA1L charac-terized in a previous study.[69] Thus, we assert that our Spot-ID method may provide more reliable results for submitochondrial protein localization and membrane topology analysis than conventional biochemical assays.

Technically, our Spot-ID approach is conceptually similar to chemical modification methods that have been employed for membrane protein topology identification[70] or for probing solvent accessible residues on the protein surface[71] using reactive biotin-probes.[19] In contrast to the radical probe in the APEX system, however, conventional probes such as biotin ester or biotin maleimide have a much longer lifetime in aqueous solution ($t_{1/2}$ = 15 min to 2 h),[72] thus, these probes are not compatible for spatiotemporal protein labeling in a specific intracellular compartment of the live cell. Therefore, to the best of our knowledge, our approach might be the only currently available method to identify the proteomic topology of

mitochondrial membrane proteins in a high-throughput manner. Furthermore, our Spot-ID method can be potentially employed to map other types of subcellular proteomic topology in live cells.

In conclusion, we developed a new approach to map phenoxyl-radical labeled sites using a newly designed chemical probe for APEX labeling. We found that our new method, Spot-ID, provided unbiased mapping results with higher spatial resolution than the previous indirect identification approach. Furthermore, the labeled sites on the protein provided valuable structural information, such the topological orientation of membrane proteins or surface-exposed residues of endogenous proteins in live cells, which was largely unobtainable by traditional chemical or biological methods. In this study, we were able to confirm and propose the membrane topologies of 135 IMM proteins and 4 beta-barrel OMM proteins. Our proposed topology of subunits of OxPhos complex are consistent with that of macromolecular complexes previously identified by EM or X-ray crystallography, which supports our proposed topologies for other mitochondrial proteins. We also found a positive correlation between the MS intensity of labeled peptides and their solvent-exposed level in the crystal structure. Overall, all of these data support that our approach can identify the in vivo structural topology of the subcellular proteome in live cells.

■ EXPERIMENTAL PROCEDURES

Desthiobiotin-Phenol Synthesis. Desthiobiotin (100 mg) was dissolved in 2 mL DMSO (dimethyl sulfoxide) at room temperature. 1.1 equiv of HATU (2-(7-aza-1H-benzotriazole-1-yl)-1,1,3,3-tetrame-thyluronium hexafluorophosphate) and 2.0 equiv of DIPEA (N,N-diisopropylethylamine) were added into the solution. The mixture was stirred for 10 min at room temperature. Then 2.0 equiv of the tyramine was added. The reaction mixture was stirred overnight at room temperature. Detail product purification method and chemical characterization data are shown in Supporting Information.

Stable Cell Line Selection and Culturing. Flp-In T-REx 293 cells (Life Technologies) were transfected using Lipofectamine 2000 (Life Technologies), typically with 20 μL Lipofectamine 2000 and 4000 ng plasmid (9:1 = pOG44:pCDNA5) per T25 flask. After 24 h, cells were cultured and selected with hygromycin B (100−200 μg/mL) for 2−3 weeks. To induce the protein expression in stable cells, cells were treated with 100 ng/mL doxycycline. Cells were desthiobiotin-phenol-labeled and lysed 18−24 h after induction. Detail information is shown in Supporting Information.

Desthiobiotin-Phenol Labeling in Stably Expressed APEX Cell Line. The stable cells were incubated with 250 μM desthiobiotin-phenol or biotin-phenol. at 37 °C under 5% CO_2 for 30 min. Afterward, 750 μL of 10 mM H_2O_2 (diluted from 30% H_2O_2, Sigma-Aldrich H1009) was added to each flask, for a final concentration of 1 mM H_2O_2, and the flasks were gently agitated for 1 min at room temperature. The reaction was then quenched by adding 7.5 mL of DPBS containing 10 mM Trolox, 20 mM sodium azide, and 20 mM sodium ascorbate to each flask. Then, cells were washed three times with cold quenching solution (DPBS containing 5 mM Trolox, 10 mM sodium azide, and 10 mM sodium ascorbate) and lysed with 1.5 mL RIPA lysis buffer (50 mM Tris, 150 mM NaCl, 0.1% SDS, 0.5% sodium deoxycholate, 1% Triton X-100), 1 × protease cocktail, 1 mM PMSF (phenylmethylsulfonyl fluoride), 10 mM sodium azide, 10 mM sodium ascorbate, and 5 mM Trolox for 10 min at 4 °C. Lysates were clarified by centrifugation at 15 000g for 10 min at 4 °C. Detail information is shown in Supporting Information.

Labeled Peptide Enrichment. For removal of unreacted free desthiobiotin-phenol or biotin-phenol, cell lysates was moved into Amicon filter (Merck Millipore, 10 kDa-off) followed by centrifugation at 7500g for 15 min at 4 °C. PBS (phosphate-buffered saline) containing 1 mM PMSF and 1 × protease cocktail was added up to 4

mL followed by centrifugation three more times. Finally, the cell lysates was transferred to an Eppendorf tube and mixed with 300 μL of streptavidin beads (Pierce). The sample was rotated for 1 h at room temperature and washed twice with PBS. After removing the PBS, 100 μL of denaturing solution (6 M urea, 2 M thiourea, 10 mM HEPES) was added and reduced using 20 μL of 100 mM DTT (dithiothreitol) in 50 mM ammonium bicarbonate (ABC) buffer for 60 min at 56 °C using a Thermomixer (Eppendorf). Protein alkylation was performed by adding 35 μL of 300 mM iodoacetamide in 50 mM ABC buffer with shaking in the dark for 30 min. Afterward, trypsin gold (Promega) was added.to the solution and incubated at 37 °C with shaking for overnight. Afterward, formic acid was added to terminate the trypsin reaction and the beads were washed with PBS four times and eluted by boiling at 95 °C for 10 min after adding 250 μL of 95% formamide, 10 mM EDTA, pH 8.2. Eluted peptide samples was desalted with Varian Bond ELUT (Agilent, 12109301) and home-made column. Detailed information for desalting and LC−MS/MS is described in Supporting Information.

LC−MS/MS Data Processing. All MS/MS data were searched by MS-GF+ algorithm[73,74] (v.9979) and MaxQuant (version 1.5.3.30) with Andromeda[75] search engine at 10 ppm of precursor ion mass tolerance against the SwissProt *Homo sapiens* proteome database (20199 entries, UniProt (http://www.uniprot.org/)). The False discovery rate (FDR) was set at <1% for peptide spectrum match including unlabeled peptides for both search algorithms. FDR less than 1% was obtained for unique labeled peptide and unique labeled protein level as well. The extracted ion chromatogram (XIC) was plotted by Qual Browser in Xcalibur software (Thermo Scientific). Detail information is described in Supporting Information.

ASSOCIATED CONTENT

Ⓢ Supporting Information

The Supporting Information is available free of charge on the ACS Publications website at DOI: 10.1021/jacs.6b10418.

> Detail information on plasmid constructs, bioinformatics analysis of TMEM261, transiently expressed APEX2 sample preparation, Supporting result, Supporting analysis and discussion; Representative spectra of DBP-labeled peptides (PDF)
> Data Set S1 (XLSX)
> Data Set S2 (XLSX)
> Data Set S3 (XLSX)
> Data Set S4 (XLSX)
> Data Set S5 (XLSX)
> Data Set S6 (XLSX)
> Data Set S7 (XLSX)

AUTHOR INFORMATION

Corresponding Authors
*jkseo6998@unist.ac.kr
*jongseokim@snu.ac.kr
*rhee@unist.ac.kr

ORCID Ⓞ
Hyun-Woo Rhee: 0000-0002-3817-3455

Notes

The authors declare the following competing financial interest(s): Ulsan National Institute of Science and Technology and Institute of Basic Science are seeking to file a patent application covering part of the information contained in the paper.

ACKNOWLEDGMENTS

REFERENCES

(1) Cogliati, S.; Frezza, C.; Soriano, M. E.; Varanita, T.; Quintana-Cabrera, R.; Corrado, M.; Cipolat, S.; Costa, V.; Casarin, A.; Gomes, L. C.; Perales-Clemente, E.; Salviati, L.; Fernandez-Silva, P.; Enriquez, J. A.; Scorrano, L. *Cell* **2013**, *155*, 160−171.

(2) Cogliati, S.; Enriquez, J. A.; Scorrano, L. *Trends Biochem. Sci.* **2016**, *41*, 261−273.

(3) Tsukihara, T.; Aoyama, H.; Yamashita, E.; Tomizaki, T.; Yamaguchi, H.; ShinzawaItoh, K.; Nakashima, R.; Yaono, R.; Yoshikawa, S. *Science* **1996**, *272*, 1136−1144.

(4) Zhang, Z. L.; Huang, L. S.; Shulmeister, V. M.; Chi, Y. I.; Kim, K. K.; Hung, L. W.; Crofts, A. R.; Berry, E. A.; Kim, S. H. *Nature* **1998**, *392*, 677−684.

(5) Sun, F.; Huo, X.; Zhai, Y. J.; Wang, A. J.; Xu, J. X.; Su, D.; Bartlam, M.; Rao, Z. H. *Cell* **2005**, *121*, 1043−1057.

(6) Zhu, J.; Vinothkumar, K. R.; Hirst, J. *Nature* **2016**, *536*, 354−8.

(7) Neupert, W. *Annu. Rev. Biochem.* **1997**, *66*, 863−917.

(8) Harner, M.; Korner, C.; Walther, D.; Mokranjac, D.; Kaesmacher, J.; Welsch, U.; Griffith, J.; Mann, M.; Reggiori, F.; Neupert, W. *EMBO J.* **2011**, *30*, 4356−4370.

(9) Kamer, K. J.; Mootha, V. K. *Nat. Rev. Mol. Cell Biol.* **2015**, *16*, 545−553.

(10) Bogenhagen, D. F.; Rousseau, D.; Burke, S. *J. Biol. Chem.* **2008**, *283*, 3665−3675.

(11) Chen, X. J.; Wang, X. W.; Kaufman, B. A.; Butow, R. A. *Science* **2005**, *307*, 714−717.

(12) Lewis, S. C.; Uchiyama, L. F.; Nunnari, J. *Science* **2016**, *353*, aaf5549.

(13) Wallace, D. C. *Nat. Rev. Cancer* **2012**, *12*, 685−698.

(14) Gerbitz, K. D.; Gempel, K.; Brdiczka, D. *Diabetes* **1996**, *45*, 113−126.

(15) Lin, M. T.; Beal, M. F. *Nature* **2006**, *443*, 787−795.

(16) Fulda, S.; Galluzzi, L.; Kroemer, G. *Nat. Rev. Drug Discovery* **2010**, *9*, 447−464.

(17) Arce, P. M.; Khdour, O. M.; Goldschmidt, R.; Armstrong, J. S.; Hecht, S. M. *ACS Med. Chem. Lett.* **2011**, *2*, 608−613.

(18) Foskett, J. K.; Madesh, M. *Biochem. Biophys. Res. Commun.* **2014**, *449*, 377−383.

(19) Bennett, K. L.; Matthiesen, T.; Roepstorff, P. *Methods Mol. Biol.* **2000**, *146*, 113−131.

(20) Deribe, Y. L.; Pawson, T.; Dikic, I. *Nat. Struct. Mol. Biol.* **2010**, *17*, 666−672.

(21) Rhee, H. W.; Zou, P.; Udeshi, N. D.; Martell, J. D.; Mootha, V. K.; Carr, S. A.; Ting, A. Y. *Science* **2013**, *339*, 1328−1331.

(22) Hung, V.; Zou, P.; Rhee, H. W.; Udeshi, N. D.; Cracan, V.; Svinkina, T.; Carr, S. A.; Mootha, V. K.; Ting, A. Y. *Mol. Cell* **2014**, *55*, 332−341.

(23) Mick, D. U.; Rodrigues, R. B.; Leib, R. D.; Adams, C. M.; Chien, A. S.; Gygi, S. P.; Nachury, M. V. *Dev. Cell* **2015**, *35*, 497−512.

(24) Jing, J.; He, L.; Sun, A.; Quintana, A.; Ding, Y.; Ma, G.; Tan, P.; Liang, X.; Zheng, X.; Chen, L.; Shi, X.; Zhang, S. L.; Zhong, L.; Huang, Y.; Dong, M. Q.; Walker, C. L.; Hogan, P. G.; Wang, Y.; Zhou, Y. *Nat. Cell Biol.* **2015**, *17*, 1339−1347.

(25) Ghesquiere, B.; Jonckheere, V.; Colaert, N.; Van Durme, J.; Timmerman, E.; Goethals, M.; Schymkowitz, J.; Rousseau, F.; Vandekerckhove, J.; Gevaert, K. *Mol. Cell. Proteomics* **2011**, *10*, M110.006866.

(26) Nam, J. S.; Kang, M. G.; Kang, J.; Park, S. Y.; Lee, S. J.; Kim, H. T.; Seo, J. K.; Kwon, O. H.; Lim, M. H.; Rhee, H. W.; Kwon, T. H. *J. Am. Chem. Soc.* **2016**, *138*, 10968−10977.

(27) Melville, D. B.; Dittmer, K.; Brown, G. B.; Vigneaud, D. U. V. *Science* **1943**, *98*, 497−499.

(28) Hirsch, J. D.; Eslamizar, L.; Filanoski, B. J.; Malekzadeh, N.; Haugland, R. P.; Beechem, J. M.; Haugland, R. P. *Anal. Biochem.* **2002**, *308*, 343−357.

(29) Burnley, B. T.; Afonine, P. V.; Adams, P. D.; Gros, P. *eLife* **2012**, *1*, e00311.

(30) Lam, S. S.; Martell, J. D.; Kamer, K. J.; Deerinck, T. J.; Ellisman, M. H.; Mootha, V. K.; Ting, A. Y. *Nat. Methods* **2015**, *12*, 51−54.

(31) Leary, S. C.; Cobine, P. A.; Kaufman, B. A.; Guercin, G. H.; Mattman, A.; Palaty, J.; Lockitch, G.; Winge, D. R.; Rustin, P.; Horvath, R.; Shoubridge, E. A. *Cell Metab.* **2007**, *5*, 9−20.

(32) Martell, J. D.; Deerinck, T. J.; Sancak, Y.; Poulos, T. L.; Mootha, V. K.; Sosinsky, G. E.; Ellisman, M. H.; Ting, A. Y. *Nat. Biotechnol.* **2012**, *30*, 1143−1148.

(33) Wang, G.; Chen, H. W.; Oktay, Y.; Zhang, J.; Allen, E. L.; Smith, G. M.; Fan, K. C.; Hong, J. S.; French, S. W.; McCaffery, J. M.; Lightowlers, R. N.; Morse, H. C.; Koehler, C. M.; Teitell, M. A. *Cell* **2010**, *142*, 456−467.

(34) Hajek, P.; Chomyn, A.; Attardi, G. *J. Biol. Chem.* **2007**, *282*, 5670−5681.

(35) Balsa, E.; Marco, R.; Pereles-Clemente, E.; Szklarczyk, R.; Calvo, E.; Landazuri, M. O.; Enriquez, J. A. *Cell Metab.* **2012**, *16*, 378−386.

(36) Hebert-Chatelain, E.; Jose, C.; Cortes, N. G.; Dupuy, J. W.; Rocher, C.; Dachary-Prigent, J.; Letellier, T. *Biochim. Biophys. Acta, Bioenerg.* **2012**, *1817*, 718−725.

(37) Rottgers, K.; Zufall, N.; Guiard, B.; Voos, W. *J. Biol. Chem.* **2002**, *277*, 45829−45837.

(38) Lee, S. Y.; Kang, M. G.; Park, J. S.; Lee, G.; Ting, A. Y.; Rhee, H. W. *Cell Rep.* **2016**, *15*, 1837−1847.

(39) Calvo, S. E.; Clauser, K. R.; Mootha, V. K. *Nucleic Acids Res.* **2016**, *44*, D1251−1257.

(40) Chandra, N. C.; Spiro, M. J.; Spiro, R. G. *J. Biol. Chem.* **1998**, *273*, 19715−19721.

(41) Rowland, A. A.; Voeltz, G. K. *Nat. Rev. Mol. Cell Biol.* **2012**, *13*, 607−615.

(42) Galluzzi, L.; Kepp, O.; Kroemer, G. *Nat. Rev. Mol. Cell Biol.* **2012**, *13* (12), 780−788.

(43) Kim, S. G.; Hoffman, G. R.; Poulogiannis, G.; Buel, G. R.; Jang, Y. J.; Lee, K. W.; Kim, B. Y.; Erikson, R. L.; Cantley, L. C.; Choo, A. Y.; Blenis, J. *Mol. Cell* **2013**, *49*, 172−185.

(44) Cagin, U.; Enriquez, J. A. *Int. J. Biochem. Cell Biol.* **2015**, *63*, 10−15.

(45) Tan, K.; Fujimoto, M.; Takii, R.; Takaki, E.; Hayashida, N.; Nakai, A. *Nat. Commun.* **2015**, *6*, 6580.

(46) Wu, J.; Liu, S.; Liu, G.; Dombkowski, A.; Abrams, J.; Martin-Trevino, R.; Wicha, M. S.; Ethier, S. P.; Yang, Z. Q. *Oncogene* **2012**, *31*, 333−341.

(47) Zerbes, R. M.; Bohnert, M.; Stroud, D. A.; von der Malsburg, K.; Kram, A.; Oeljeklaus, S.; Warscheid, B.; Becker, T.; Wiedemann, N.; Veenhuis, M.; van der Klei, I. J.; Pfanner, N.; van der Laan, M. *J. Mol. Biol.* **2012**, *422*, 183−191.

(48) Cserzo, M.; Eisenhaber, F.; Eisenhaber, B.; Simon, I. *Protein Eng., Des. Sel.* **2002**, *15*, 745−752.

(49) Jenkins, K.; Khoo, J. J.; Sadler, A.; Piganis, R.; Wang, D.; Borg, N. A.; Hjerrild, K.; Gould, J.; Thomas, B. J.; Nagley, P.; Hertzog, P. J.; Mansell, A. *Immunol. Cell Biol.* **2013**, *91*, 321−330.

(50) Marques, E. J.; Carneiro, C. M.; Silva, A. S.; Krasilnikov, O. V. *Biochim. Biophys. Acta, Biomembr.* **2004**, *1661*, 68−77.

(51) McDonald, B. M.; Wydro, M. M.; Lightowlers, R. N.; Lakey, J. H. *FEBS Lett.* **2009**, *583*, 739−742.

(52) Tomasello, M. F.; Guarino, F.; Reina, S.; Messina, A.; De Pinto, V. *PLoS One* **2013**, *8*, e81522.

(53) Choudhary, O. P.; Paz, A.; Adelman, J. L.; Colletier, J. P.; Abramson, J.; Grabe, M. *Nat. Struct. Mol. Biol.* **2014**, *21*, 626−632.

(54) Michaud, M.; Ubrig, E.; Filleur, S.; Erhardt, M.; Ephritikhine, G.; Marechal-Drouard, L.; Duchene, A. M. *Proc. Natl. Acad. Sci. U. S. A.* **2014**, *111*, 8991−8996.

(55) Kozjak, V.; Wiedemann, N.; Milenkovic, D.; Lohaus, C.; Meyer, H. E.; Guiard, B.; Meisinger, C.; Pfanner, N. *J. Biol. Chem.* **2003**, *278*, 48520−48523.

(56) Ujwal, R.; Cascio, D.; Colletier, J. P.; Faham, S.; Zhang, J.; Toro, L.; Ping, P. P.; Abramson, J. *Proc. Natl. Acad. Sci. U. S. A.* **2008**, *105*, 17742−17747.

(57) Schredelseker, J.; Paz, A.; Lopez, C. J.; Altenbach, C.; Leung, C. S.; Drexler, M. K.; Chen, J. N.; Hubbell, W. L.; Abramson, J. *J. Biol. Chem.* **2014**, *289*, 12566−12577.

(58) Hiller, S.; Abramson, J.; Mannella, C.; Wagner, G.; Zeth, K. *Trends Biochem. Sci.* **2010**, *35*, 514−521.

(59) Dimmer, K. S.; Navoni, F.; Casarin, A.; Trevisson, E.; Endele, S.; Winterpacht, A.; Salviati, L.; Scorrano, L. *Hum. Mol. Genet.* **2008**, *17*, 201−14.

(60) Haque, M. E.; Elmore, K. B.; Tripathy, A.; Koc, H.; Koc, E. C.; Spremulli, L. L. *J. Biol. Chem.* **2010**, *285*, 28353−28362.

(61) Martell, J. D.; Deerinck, T. J.; Sancak, Y.; Poulos, T. L.; Mootha, V. K.; Sosinsky, G. E.; Ellisman, M. H.; Ting, A. Y. *Nat. Biotechnol.* **2012**, *30*, 1143−8.

(62) Claros, M. G.; Vincens, P. *Eur. J. Biochem.* **1996**, *241*, 779−786.

(63) Rees, D. M.; Leslie, A. G. W.; Walker, J. E. *Proc. Natl. Acad. Sci. U. S. A.* **2009**, *106*, 21597−21601.

(64) Chong, S. H.; Ham, S. *Acc. Chem. Res.* **2015**, *48*, 956−965.

(65) Dickson, A.; Brooks, C. L. *J. Am. Chem. Soc.* **2013**, *135*, 4729−4734.

(66) Stiller, S. B.; Hopker, J.; Oeljeklaus, S.; Schutze, C.; Schrempp, S. G.; Vent-Schmidt, J.; Horvath, S. E.; Frazier, A. E.; Gebert, N.; van der Laan, M.; Bohnert, M.; Warscheid, B.; Pfanner, N.; Wiedemann, N. *Cell Metab.* **2016**, *23*, 901−908.

(67) Darshi, M.; Mendiola, V. L.; Mackey, M. R.; Murphy, A. N.; Koller, A.; Perkins, G. A.; Ellisman, M. H.; Taylor, S. S. *J. Biol. Chem.* **2011**, *286*, 2918−2932.

(68) Kim, H.; Melen, K.; Osterberg, M.; von Heijne, G. *Proc. Natl. Acad. Sci. U. S. A.* **2006**, *103*, 11142−11147.

(69) Sato, T.; Mihara, K. *J. Biol. Chem.* **2009**, *284*, 14819−14827.

(70) Song, J. M.; Midson, C.; Blachly-Dyson, E.; Forte, M.; Colombini, M. *J. Biol. Chem.* **1998**, *273*, 24406−24413.

(71) Suckau, D.; Mak, M.; Przybylski, M. *Proc. Natl. Acad. Sci. U. S. A.* **1992**, *89*, 5630−5634.

(72) Grumbach, I. M.; Veh, R. W. *J. Immunol. Methods* **1991**, *140*, 205−210.

(73) Kim, S.; Mischerikow, N.; Bandeira, N.; Navarro, J. D.; Wich, L.; Mohammed, S.; Heck, A. J.; Pevzner, P. A. *Mol. Cell. Proteomics* **2010**, *9*, 2840−2852.

(74) Kim, S.; Pevzner, P. A. *Nat. Commun.* **2014**, *5*, 5277.

(75) Cox, J.; Neuhauser, N.; Michalski, A.; Scheltema, R. A.; Olsen, J. V.; Mann, M. *J. Proteome. Res.* **2011**, *10*, 1794−1805.